A multispectral and polarization-selective surface-plasmon resonant midinfrared detector

Jessie Rosenberg,[1,a)] Rajeev V. Shenoi,[2] Thomas E. Vandervelde,[2] Sanjay Krishna,[2,b)] and Oskar Painter[1,c)]
[1]*Thomas J. Watson, Sr., Laboratory of Applied Physics, California Institute of Technology, Pasadena, California 91125, USA*
[2]*Department of ECE, Center for High Technology Materials, University of New Mexico, Albuquerque, New Mexico 87106, USA*

(Received 15 July 2009; accepted 10 September 2009; published online 19 October 2009)

We demonstrate a multispectral polarization sensitive midinfrared dots-in-a-well photodetector utilizing surface-plasmonic resonant elements, with tailorable frequency response and polarization selectivity. The resonant responsivity of the surface-plasmon detector shows an enhancement of up to five times that of an unpatterned control detector. As the plasmonic resonator involves only surface patterning of the top metal contact, this method is independent of light-absorbing material and can easily be integrated with current focal plane array processing for imaging applications.
 [doi:10.1063/1.3244204]

Multicolor midinfrared imaging is a highly desirable technology in a number of applications such as night vision, missile tracking, medical diagnostics, and environmental monitoring.[1] The current dominant technologies in the field of multispectral imaging rely on the use of either a broadband focal plane array (FPA) with a spinning filter wheel in front of it,[2] or a bank of FPAs with a dispersive element such as a grating or prism to separate light of different frequencies. These methods are limited by the often high cost and complexity of such systems. However, if spectral sensitivity could be encoded at the pixel level within a single FPA, multispectral detection would become much more practical. In addition, the use of pixel-integrated resonators for spectral sensitivity can dramatically increase the efficiency of the detector due to the many passes light makes within the resonator.

The most common methods for pixel-level encoding utilize epitaxially defined dielectric Fabry–Pérot cavities[3–5] or lithographically patterned gratings,[6] but these can be difficult to integrate into standard FPA processing. Previously pixel-integrated resonant detectors utilizing dielectric photonic crystals (PCs),[7,8] deep-etched plasmonic PCs,[9] and metallic Fabry–Pérot cavities[10] have been shown in the midinfrared region, as well as plasmonic color-selective gratings in the visible region.[11,12] Here we design and demonstrate midinfrared frequency and polarization-specific plasmonic PC detector pixels in dots-in-a-well (DWELL) photodetector material[13] utilizing a shallow etch design extending only through the top plasmonic metal layer. This resonator design can be used with any detector material system, does not introduce any etching damage to the detector active material, and adds only one lithography step to current FPA processing techniques. Finite element modeling reproduces the experimentally measured spectral response, and also shows good agreement with the measured level of responsivity enhancement at the plasmonic cavity resonant wavelengths.

The resonant cavity used in this work consists of a single layer of metal with etched square holes in a square lattice periodic array. A representation of several lattice constants of the device structure is shown in Fig. 1(a). The plasmonic layer provides vertical confinement, confining the optical mode with a maximum at the surface of the metal [Figs. 1(d) and 1(e)], while the etched air-holes create a PC pattern to confine the light in plane. This combined resonator design provides full three-dimensional confinement, significantly increasing the amount of time light spends within the detector active region, and therefore enhancing the probability of detection. Due to the strong index contrast between the surface plasmon[14] mode beneath the metal regions and the dielectric-confined mode beneath the air holes, this plasmonic PC grating is strong enough to generate an in-plane confined resonant mode without etching into the detector active material,[15,16] allowing a resonator to be fabricated without damaging or removing active material. A detailed numerical and symmetry analysis[17] shows that the two degenerate dipolelike in-plane modes of the structure [Figs. 1(d)–1(f)] couple most easily from free space. As these two modes couple to orthogonal polarizations of incoming light, a stretch of the PC lattice breaks the degeneracy, splitting their resonance frequencies and thus achieving high polarization selectivity.[8,18]

The finite difference time domain (FDTD) simulated active region absorption and enhancement factor (details presented in Ref. 17) are plotted versus frequency in Fig. 1(b) for a perfectly periodic structure, showing the fundamental plasmonic (degenerate) dipolelike modes at $\lambda=7.8$ μm (the two shorter wavelength resonance peaks correspond to higher-order vertical waveguide modes of the DWELL epitaxy). The series of resonance peaks near $\lambda=5.5$ μm correspond to higher-order modes of the in-plane square lattice PC. Figure 1(c) shows relevant dimensions of the structure; we define the normalized hole width as $\bar{W}=2W/(a_x+a_y)$. Field profiles along different planes for the square lattice dipolelike mode are plotted in Figs. 1(d)–1(f) over a single unit cell; the other dipole mode has the same field pattern, rotated by 90° in the x-y plane. The simulated active region absorption corresponding to this mode is 10.9%, given an approximate 2% single-pass absorption in the DWELL material, and corresponds to an expected resonant responsivity

a)Electronic mail: jessier@caltech.edu.
b)Electronic mail: skrishna@chtm.unm.edu.
c)Electronic mail: opainter@caltech.edu.

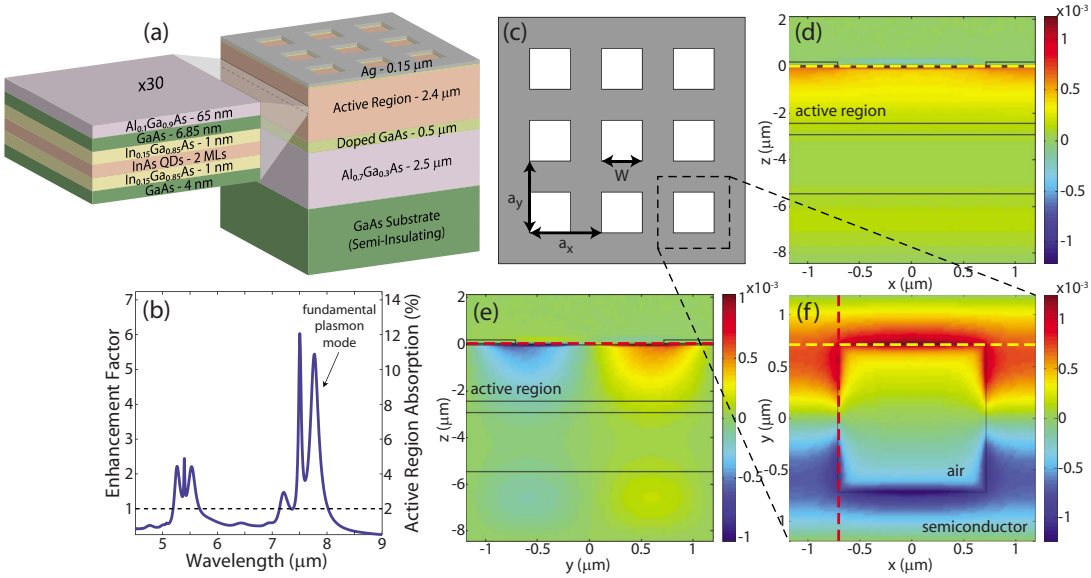

FIG. 1. (Color online) (a) A cross-section of the device structure. (b) FDTD simulated enhancement factor and active region absorption vs wavelength, based on a 2% single-pass absorption. All simulations use a structure with $a=2.38$ μm, $\bar{W}=0.6$, and metal thickness $t=150$ nm. (c) A diagram of the unstretched PC structure showing relevant dimensions. Expanded plots show the E_z mode profile for one lattice constant of one of the two dipole modes for an unstretched PC lattice in (d) the x-z plane along the hole edge, (e) the y-z plane along the hole edge, and (f) the x-y plane just beneath the metal-semiconductor interface.

enhancement of five to six times that of a control sample with no plasmonic layer or PC patterning.

To test these predictions, we fabricated the two following detector samples: sample A with a square lattice PC and sample B with a rectangular lattice PC having a lattice constant stretching ratio $a_y/a_x=1.2$. Figures 2(a)–2(c) show representative images of the fabricated devices. All of the PC patterns had the same normalized hole width ($\bar{W}\sim 0.6$), but different lattice constant values and therefore different resonant wavelengths. The spectral response of the resonant detectors was measured at 30 K using a Fourier transform infrared (FTIR) spectrometer with the patterned detector sample used in place of the standard FTIR detector. Responsivity and detectivity measurements were performed at 77 K using the experimental setup shown in Fig. 2(d). To separate out the background scattering and the frequency response of the DWELL material from the resonant enhancement, we perform data processing as shown in Fig. 3(c).

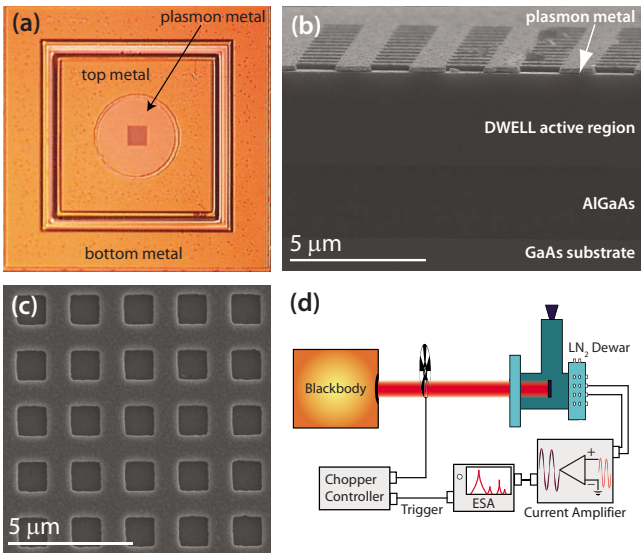

FIG. 2. (Color online) (a) Optical image of the fabricated device indicating the top, bottom, and plasmon metallizations. (b) Cross-sectional SEM of the fabricated square-lattice device. (c) SEM image of the fabricated square-lattice PC pattern on the plasmon metallization. (d) Schematic of the setup used for measuring responsivity and detectivity of the fabricated devices. The sample was illuminated with a calibrated Mikron M365 blackbody at $T=800$ K, modulated at a frequency of 400 Hz using a chopper and used to trigger the SRS 760 fast Fourier transform spectrum analyzer. The photocurrent was amplified using a SRS 570 low noise amplifier and then measured in the spectrum analyzer.

As predicted, by varying the lattice constant and symmetry of the patterned grating, we are able to tailor the wavelength and polarization response of each detector pixel. Figure 3(a) shows the resonant spectral response from a set of representative detector pixels on sample A, varying the peak wavelength response from 5.5 to 7.2 μm by choosing PC lattice constants in a range from 1.83 to 2.38 μm. The linewidth of these resonances is $\sim$0.9 μm, providing strong spectral sensitivity within the broad background DWELL response covering more than 5 μm. In addition to the fundamental surface plasmon resonant mode, we also observe a higher-order plasmon mode as predicted in Fig. 1(b), at a wavelength in good agreement with the theory. In order to generate a polarization-sensitive response, we stretch the lattice constant in one direction (sample B), splitting the resonant response into two well-separated peaks as shown in the green curve of Fig. 3(b). By varying the polarization of the incident light, we show that these two peaks correspond to orthogonal linear polarization directions of incoming light, as represented by the blue and red curves of Fig. 3(b). The high polarization extinction between the two curves indicates clearly the strong polarization dependence in our device. The experimentally measured spectral peaks are broadened relative to the FDTD simulated values in Fig. 1(b) due to the finite extent of the PC pattern ($\sim$50 μm in diameter), and therefore the limited in-plane confinement.

To characterize the efficiency of the detector response and the resonant enhancement, we define and measure the responsivity and detectivity of samples A and B as follows.

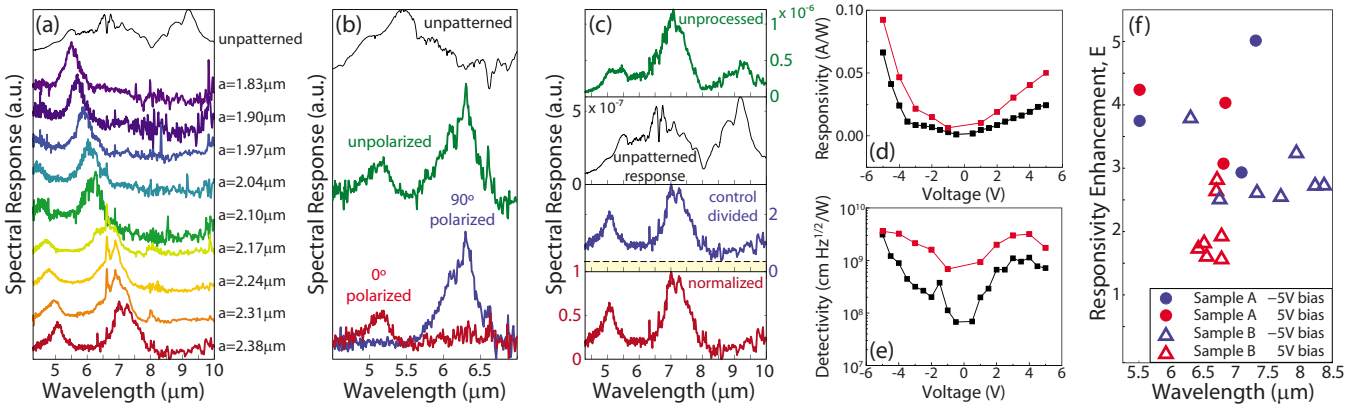

FIG. 3. (Color online) (a) Normalized spectral response from square lattice devices at a bias of 5 V, indicating tuning of peak wavelength with the lattice constant. (b) Normalized spectral response from a rectangular lattice device (a_x=1.65 μm, a_y=2.02 μm) at a bias of −5 V, showing the response to unpolarized light (green) and beneath, the response to light polarized at 0° (red) and 90° (blue) relative to the x-axis of the lattice. (c) Data processing of the a=2.38 μm device response. The unprocessed data (green) is divided by the unpatterned DWELL response, and the background scattering (yellow) is subtracted and normalized, giving the final spectral response (red) that is plotted in (a) and (b). (d) Measured responsivity and (e) detectivity of a stretched lattice device with a_x=1.78 μm and a_y=2.16 μm (red) and a control device (black). (f) Measured peak responsivity enhancement E vs resonant device wavelength for two samples at positive and negative bias.

The peak responsivity was computed using the expression:

$$R_p = \frac{I_0}{\int_{\lambda_1}^{\lambda_2} R_N(\lambda) L_e(\lambda, T) A_s A_d \frac{tF_F}{r^2} d\lambda}, \quad (1)$$

where $R_N(\lambda)$, I_0, L_e, T, A_s, and A_d are the normalized spectral response, measured photocurrent, black body spectral excitance, black body source temperature, area of the source, and area of the detector, and r, t, and F_F are the distance between the source and the detector, the transmission of the window, and the geometrical form factor, respectively. The lower and upper wavelength bounds of the detector response are given by λ_1 and λ_2. The detectivity is then $D^*=R_p\sqrt{A_d \Delta f}/i_n$, where A_d is the detector area, Δf is the noise equivalent bandwidth of our measurement, and i_n is the noise current.

Compared to a control (unpatterned) sample, the plasmonic PC patterned devices provide a strong enhancement of responsivity and a corresponding increase in detectivity across an applied bias range from −5 to 5 V, as shown in Figs. 3(d) and 3(e). The enhancement factor E is defined as $E=R(\lambda_i)/R_c(\lambda_i)$, where $R(\lambda_i)$ is the responsivity of the patterned detector and $R_c(\lambda_i)$ is the responsivity of the control sample, both at the resonant wavelength. In Fig. 3(f), we show enhancement factors reaching as high as five times for sample A and four times for sample B. With further improvement to the free-space coupling[19] and the cavity quality factor through incorporation of a bottom metal layer forming a double-metal cavity,[17] we estimate this factor could be improved by another factor of 5.

In summary, we have designed and fabricated a multispectral midinfrared photodetector utilizing a plasmonic resonator for frequency sensitivity, polarization splitting, and responsivity enhancement. We demonstrate control over the peak wavelength response of the detector pixels, strong polarization selectivity, and resonant responsivity enhancements of up to five times. Though we chose the valuable midinfrared region for this demonstration, the resonator design can be extended for use at wavelengths from the terahertz to the visible with suitable scaling of the PC holes. As it involves only a surface patterning, it can be used with various light absorbing materials and detector designs. The single-metal waveguide structure shown here can also be extended to a double-metal structure that would readily integrate with current FPA processing, and would enable higher quality factor modes with better active region confinement and thus higher frequency selectivity and responsivity enhancement.

The authors would like to thank R. Perahia for help in the initial device processing. This work was supported by the AFOSR through Grant No. FA9550-06-1-0443 and MURI Grant No. FA9550-04-1-0434, the AFRL through Grant No. FA9453-07-C-0171, and the IC post-doctoral program.

[1] A. Rogalski, Opto-Electron. Rev. **16**, 458 (2008).
[2] M. L. Althouse and C. I. Chang, Opt. Eng. **30**, 1725 (1991).
[3] H. Huang, Y. Huang, X. Wang, Q. Wang, and X. Ren, IEEE Photonics Technol. Lett. **16**, 245 (2004).
[4] Q. Han, X. H. Yang, Z. C. Niu, H. Q. Ni, Y. Q. Xu, S. Y. Zhang, Y. Du, L. H. Peng, H. Zhao, C. Z. Tong, R. H. Wu, and Q. M. Wang, Appl. Phys. Lett. **87**, 111105 (2005).
[5] R. S. Attaluri, J. Shao, K. T. Posani, S. J. Lee, J. S. Brown, A. Stintz, and S. Krishna, J. Vac. Sci. Technol. B **25**, 1186 (2007).
[6] K. W. Goossen and S. A. Lyon, Appl. Phys. Lett. **47**, 1257 (1985).
[7] K. T. Posani, V. Tripathi, S. Annamalai, N. R. Weisse-Bernstein, S. Krishna, R. Perahia, O. Crisafulli, and O. J. Painter, Appl. Phys. Lett. **88**, 151104 (2006).
[8] J. K. Yang, M. K. Seo, I. K. Hwang, S. B. Kim, and Y. H. Lee, Appl. Phys. Lett. **93**, 211103 (2008).
[9] R. V. Shenoi, D. A. Ramirez, Y. Sharma, R. S. Attaluri, J. Rosenberg, O. J. Painter, and S. Krishna, Proc. SPIE **6713**, 67130P (2007).
[10] X. Hu, M. Li, Z. Ye, W. Y. Leung, K. M. Ho, and S. Y. Lin, Appl. Phys. Lett. **93**, 241108 (2008).
[11] E. Laux, C. Genet, T. Skauli, and T. W. Ebbesen, Nat. Photonics **2**, 161 (2008).
[12] J. S. White, G. Veronis, Z. Yu, E. S. Barnard, A. Chandran, S. Fan, and M. L. Brongersma, Opt. Lett. **34**, 686 (2009).
[13] R. V. Shenoi, R. S. Attaluri, A. Siroya, J. Shao, Y. D. Sharma, A. Stintz, T. E. Vandervelde, and S. Krishna, J. Vac. Sci. Technol. B **26**, 1136 (2008).
[14] H. Raether, *Surface Plasmons on Smooth and Rough Surfaces and on Gratings* (Springer, New York, 1988).
[15] J. B. Pendry, L. Martin-Moreno, and F. J. Garcia-Vidal, Science **305**, 847 (2004).
[16] M. Bahriz, V. Moreau, R. Colombelli, O. Crisafulli, and O. Painter, Opt. Express **15**, 5948 (2007).
[17] J. Rosenberg, R. V. Shenoi, S. Krishna, and O. Painter, arXiv: 0910.2801v1.
[18] O. Painter and K. Srinivasan, Opt. Lett. **27**, 339 (2002).
[19] M. Cai, O. Painter, and K. J. Vahala, Phys. Rev. Lett. **85**, 74 (2000).